Advances in Science and Technology Research Journal

Volume 13, Issue 3, September 2019, pages 179–185
https://doi.org/10.12913/22998624/111965

Received: 2019.07.15
Revised: 2019.07.30
Accepted: 2019.08.15
Available online: 2019.08.31

Comparing of Microhardness of the Stellite 6 Cobalt Alloy Implanted with 175 keV Mn^+ Ions and 120 keV N^+ Ions

Mariusz Kamiński[1*], Piotr Budzyński[1], Mirosław Szala[2], Marcin Turek[3]

[1] Department of Automotive Vehicles, Faculty of Mechanical Engineering, Lublin University of Technology, Nadbystrzycka str. 36, 20-618 Lublin, Poland

[2] Department of Materials Engineering, Faculty of Mechanical Engineering, Lublin University of Technology, Nadbystrzycka str. 36, 20-618 Lublin, Poland

[3] Institute of Physics, M. Curie-Skłodowska University, M. Curie-Sklodowska sq. 1, 20-031 Lublin, Poland

* Corresponding author's e-mail: mariusz.kaminski@pollub.pl

ABSTRACT

Nowadays, high-precision machines require lightweight materials with very high strength. Ion implantation is used to improve the mechanical strength of the material. A further paper presents the influence of manganese and nitrogen ion implantation on changes of microhardness of the surface layer of cobalt alloy. Samples were analyzed with the SEM-EDS Phenom ProX microscope. Microhardness was assessed with the Vickers method, and the loads of 1 gf (0.00981 N) and 5 gf (0.049 N) was applied using a FM-800 from Future-Tech microhardness meter. At a load of 1 gf, the penetration depth of the implanted specimens was reached not exceeding 0.5 um. At this depth, all samples showed an increase in microhardness compared to the unimplanted sample. The highest increase in microhardness was achieved after implantation of Mn ions with dose $D=1\cdot10^{17}$ Mn^+/cm^2 and energy E=175 keV. The increased load on the indenter to 5 gf reduced the microhardness differences between implanted and unimplanted samples.

Keywords: ion implantation, Stellite 6, microhardness, cobalt alloy

INTRODUCTION

The construction of modern machines is inseparably connected with the need to develop construction materials that will allow to reducing the weight of equipment while increasing its reliability. In the case of combustion engines, such components as high-pressure fuel injectors, control valves in hydraulic systems, valves sealing the combustion chamber are responsible for the efficient operation of the entire unit. The proper strength of the surface layer plays an important role in the efficient operation of these components. Damage to the surface layer can affect the continued usability of the entire machine. Therefore, work is underway to improve the strength properties of the surface layer of materials.

One of the groups of materials used in the construction of internal combustion engines are cobalt alloys commonly referred to as Stellites. They are characterized by acid resistance, heat resistance and low susceptibility to corrosion. These features make the Stellites find their application as a material for the construction of turbochargers' rotors, flow valves, etc. Frequent use of Stellites is also found in the form of material for surfacing valve faces and valve seats [1, 2]. This results from the working conditions of valves, which are exposed to high temperatures and the presence of aggressive exhaust gases, where low thermal expansion of Stellite and acid and heat resistance are very desirable features [3]. The analysis of engine valves shows that they are also subjected to mechanical loads resulting from the continuous hitting of the valve seat against the valve seat surface. Therefore, it is also important to improve the material to achieve the required hardness and fatigue resistance. For increasing the hardness of metal alloys

various surface engineering processes can be used such as surface laser treatment [4, 5, 6], work hardening [7, 8], shoot peeing [9]. The purpose of the present paper is to investigate the effect of shot peening on the state of the surface layer and corrosion resistance of specimens made of Ti-6Al-4V titanium alloy produced in Direct Metal Laser Sintering (DMLS or application of thermally sprayed coatings [10, 11, 12]. The ion implantation process can also be used for this purpose.

Ion implantation allows to implant into the structure of the material atoms of any element, which will change the tribological and strength properties. There are many examples of improvement of material properties after ion implantation [13, 14, 15]. A great advantage is also the insignificant influence of ion implantation on the dimensions of the workpiece, so this process can be used as the last stage of production of products that already have final dimensions [16].

Besides the improvement of tribological properties, ion implantation contributes to an increase in mechanical strength. This is associated with an increase in the microhardness of the implanted element [17, 18]. The implantation process is accompanied with the appearance of compressive stresses and inclusions of nitrides, carbides, and borides. The implantation-induced hardening process depends on the type and dose of implanted ions and the temperature of the implanted material [19, 20] indicating a more confined plastic zone. Together, our observations suggest that helium-induced defects initially act as efficient obstacles to dislocation motion, but are weakened by the subsequent passage of dislocations, causing a reduction in work hardening capacity [21, 22]. It has been proven that the increase in the microhardness of the implanted material is a permanent change, retained even in the heating process [23].

Studies have been conducted so far indicating a slight increase in the microhardness of cobalt alloy Stellite 6 [24]. The nitrogen implantation with the energy of E=65 keV was performed. As the increase of microhardness was not sufficient for the practical application of ion implantation, an attempt was made to determine the influence of increased implantation energy on the changes in microhardness of the cobalt alloy. This paper presents the results of measurements of microhardness of Stellite 6 cobalt alloy implanted with N^+ ions with an energy of 120 keV and Mn^+ with the energy of 175 keV.

MATERIALS AND METHODS

Stellite was chosen for analysis due to its multiple applications as a material for a construction of the valves and valve faces. A commercial variety of Stellite 6 was chosen. The alloy comprises 27–32% Cr, 4–6% W, and 0.9–1.4% C. The samples for the analyses were taken from an ϕ14 mm-diameter rod. Sample surfaces intended for the analysis were polished in order to achieve a roughness value of Ra<0.02.

The samples were subjected to the ion implantation process. The distribution of the implanted ions and vacancies at equal sample depths was calculated with the use of SRIM programs [25]. which are often used in research of the distribution of ions in the material [26, 27, 28], and can be used as an input of SRIM codes for systematic analysis of primary radiation damage. Then the Bushehr Nuclear Power Plant (BNPP. Mn and N were the implanted elements. The implantation was carried out evenly over the entire surface of the sample. This paper presents the results of measurements of microhardness of Stellite 6 cobalt alloy implanted with N^+ ions with an energy of 120 keV and Mn^+ with the energy of 175 keV. The dose of the implanted ions varied between the samples. The values of the fluences of the implanted ions are presented in Table 1.

After ion implantation, the samples were subjected to microhardness testing. The measurement was performed using a microhardness meter FM-800 from Future-Tech. The implanted samples and the unimplanted sample were analyzed in order to compare the microhardness results. Hardness was assessed with the Vickers method and the loads *P* of 1 g (0,00981 N) and 5 g (0.049 N) was applied. A microhardness value of $HV_{0.001}$ and $HV_{0.005}$ was determined based on the measurements. In all tests the loading time was fixed at 10 s. After indentation, microphotographs of the

Table 1. Fluences of the implanted ions for individual samples

Sample	Implanted element	Fluences of implanted ions (ions/cm^2)
S-Mn1	Mn^+	$5 \cdot 10^{16}$
S-Mn2	Mn^+	$1 \cdot 10^{17}$
S-N1	N^+	$5 \cdot 10^{16}$
S-N2	N^+	$1 \cdot 10^{17}$
NN	unimplanted	

sample's surface were taken by the SEM-EDS Phenom ProX microscope. On their basis the diagonal length of imprint was determined and the value of microhardness HV was calculated. It is a common method for determining the microhardness of materials, based on the analysis of digital photos of the trace of indentation [29]. For Vickers hardness test, the indenter has a pyramidal with a square base shape with a semi-apex angle θ equal to 68° and the corresponding hardness number HV is calculated function of the actual contact area A_t between the indenter and the material as follows:

$$HV = \frac{P}{A_t} = \frac{2 \cdot P \cdot \sin\vartheta}{d^2} = 1.8544 \cdot \frac{P}{d^2}$$

The average diagonal length of the indexation area was also used to determine the depth of the imprint, based on the following equation:

$$h = \frac{d}{2 \cdot \sqrt{2} \cdot \tan\left(\frac{\vartheta}{2}\right)}$$

RESULTS AND DISCUSSION

For preliminary determination of ion implantation, a numerical simulation was performed. Typically, numerical simulations correspond well with experimental results. Figure 1a presents the calculated (predicted) distribution of manganese ions implanted at energy E = 175 keV and a fluence of D=1·10^{17} Mn$^+$/cm^2 into Stellite 6 and vacancies generated thereby. It is evident that the calculated range of the implanted manganese ions that does not exceed 0.15 µm and the maximum concentration of vacancies are noted at a depth of ~0.06 to 0.08 µm. Calculated (predicted) distribution of nitrogen ions implanted at energy E=120 keV and a fluence of D=1·10^{17} N$^+$/cm^2 into Stellite 6 and vacancies generated thereby are shown in figure 1b. The calculated range of the nitrogen ions have a greater range than manganese ions and reach a depth of about 0.25 µm. The highest concentration of nitrogen ions occurs at a depth of about 0.15 µm.

The samples were analysed for microhardness. Several measurements were carried out to obtain a reliable result. Figure 2a-2e shows a microphotographs of the surface with visible areas of indentation, taken with a load of 1 gf.

The literature data indicate that the hardness of overlay welded or cast cobalt alloys ranges from 300–700 HV. Which depends strongly on chemical composition and applied indentation load [31, 32]. X-ray diffraction (XRD. Observation of the microphotographs shows that the areas of indentation are quite diverse on the surface of each sample. This may be due to the fact that the structure of the material is multiphase and contains hard compounds of tungsten or carbon, which were mentioned in the paper [24]. The porosity of the material is also noticeable, which is visible in the form of dark spots in Figure 3. Conducted SEM-EDS spot analysis indicates that structure matrix (brighter phase – marked as A) is rich in Co and darker-like phases, marked as B, are enriched with Cr and C. In contrary to Co-rich phase, the Cr – bearing phases can be considered as hard phases which were acknowledged by hardness indentations (smaller diagonal for Cr-rich phases).

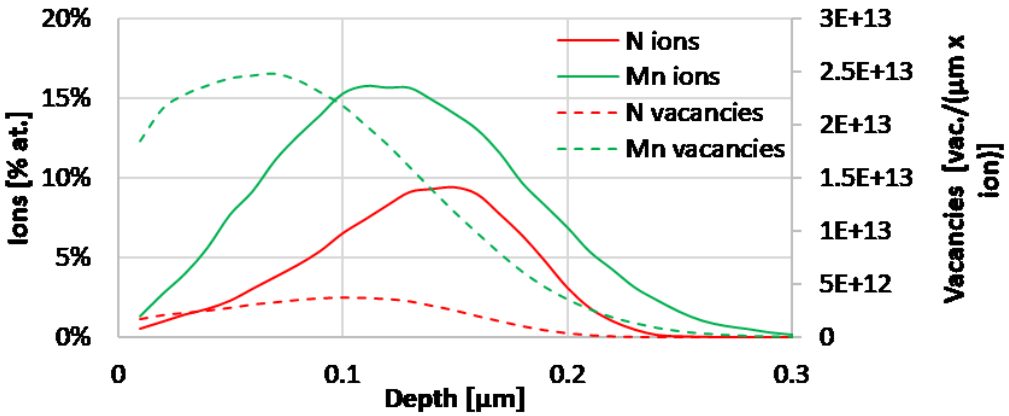

Fig. 1. Calculated distribution of ions and gaps after ion implantation of Mn$^+$ ions with E=175 keV [30]and the dose of implanted ions was set to D = 5·1016 Mn$^+$/cm^2 and D = 1·1017 Mn+/cm^2. Next, the samples were subjected to tribological tests on a pin-on-disc stand using the Nano Tribometer (NTR2 and N$^+$ ions with E=120 keV into the Stellite 6 cobalt alloy

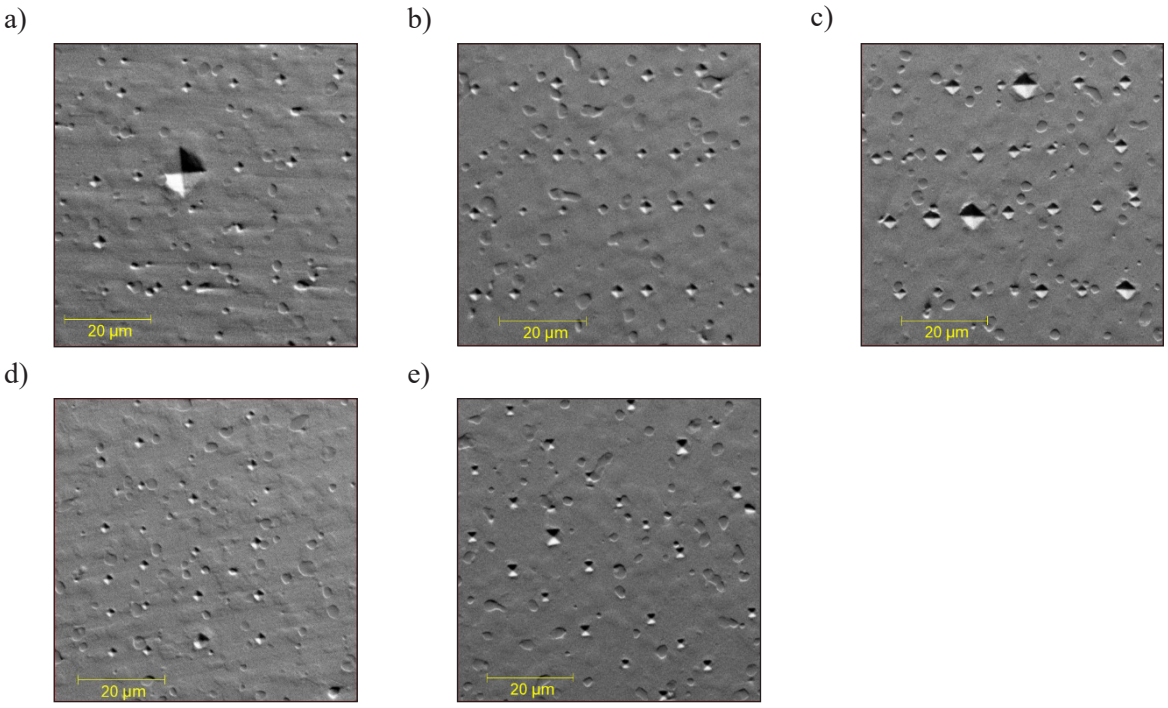

Fig. 2. SEM images of samples surface after 1gf load indentation: a) S-N2 sample; b) S-N1 sample; c) NN sample; d) S-Mn2 sample; e) S-Mn1 sample

The SEM analysis of individual indentations enabled to determine the average length of the diagonal impression of the indenter. On this basis, microhardness values were calculated. They are presented in Table 2.

The expected dispersion of the microhardness measurement results has been confirmed by the variation coefficient. The highest scattering of results was found in the case of measurements of an unimplanted sample loaded with the value of 1gf, the coefficient of variation reached 39% indicates the average variability. In the case of other series of measurements, the variation rate does not exceed 25%, so it indicates low dispersion of the results around the mean value [33].

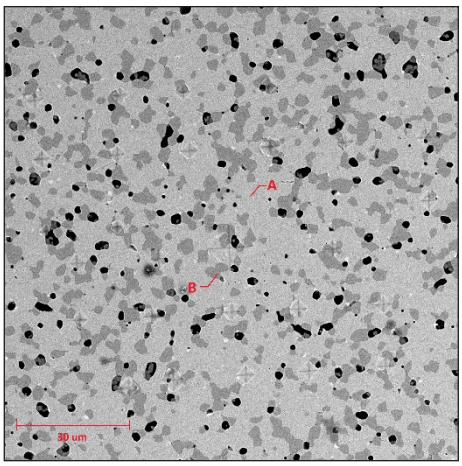

Fig. 3 SEM image of sample surface of the Stellite 6 cobalt alloy

The results of HV microhardness measurements are shown in Figure 4. It follows that the ion implantation of both Mn and N ions influenced the increase in microhardness. The Kruskal-Wallis test showed statistically significant differences in microhardness of samples implanted with Mn and N ions with doses $D=1\cdot10^{17}$ ions/cm^2 with compare to unimplanted sample. In the case of N ion implantation, this can be caused by the formation of nitrogen compounds in the material structure, which is described in the paper [34]. Manganese ion implantation does not cause the formation of new fractions, it is part of a solid solution, which was noted in [30] and the dose of implanted ions was set to D = 5·1016 Mn^+/cm^2 and D = 1·1017 Mn^+/cm^2. Next, the samples were subjected to tribological tests on a pin-on-disc stand using the Nano Tribometer NTR2. In this case, the increase in microhardness could be associated with changes in the crystalline structure of the surface layer caused by the increase in stresses resulting from a higher number of defects than in the case of nitrogen implantation, which results from the SRIM simulation. The relation between microhardness growth and structural changes of the crystalline lattice is widely described in the literature [20,

Table 2. Averaged results of microhardness measurements for each sample

Load [gf]	Sample	HV [MPa]	Standard deviation	Coefficient of variations [%]	Indent depth [μm]
1	NN	161.31	63.38	39	0.54
	S-N1	201.09	48.64	24	0.45
	S-N2	206.93	43.71	21	0.44
	S-Mn1	186.05	44.60	24	0.47
	S-Mn2	329.57	101.73	31	0.35
5	NN	354.95	67.37	19	0.73
	S-N1	367.67	69.64	19	0.72
	S-N2	363.30	70.21	19	0.73
	S-Mn1	380.79	76.18	20	0.71
	S-Mn2	372.51	66.94	18	0.71

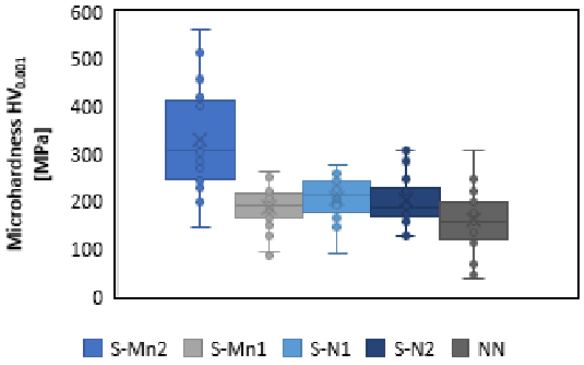

Fig. 4. Microhardness of Stellite 6 cobalt alloy determined at a load of 1 gf

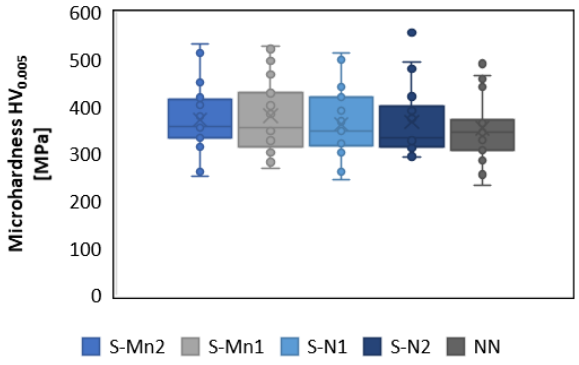

Fig. 5. Microhardness of Stellite 6 cobalt alloy determined at a load of 5 gf

35] and annealing was found to cause a reversal of this effect to the values of the unimplanted material and lower. The decrease in hardness after annealing was higher for the higher implantation dose, indicating a dose-dependent effect. Rutherford backscattering results on the sample implanted with 1.5·1017 ions cm^{-2} show a buried nitrogen layer which decreased significantly after the annealing treatment. Transmission electron microscopy data show that isolated TiN islands form directly during implantation and grow during annealing. The defect density in the implanted material is markedly reduced after annealing. The results indicate that the increase in hardness in the as-implanted material is only due to the extended lattice damage and not to TiN formation. The effect of helium-implantation-induced defects on deformation behaviour is examined by comparing spherical nano-indents in unimplanted and helium-implanted regions of a tungsten single crystal. Helium-implantation increases hardness and causes large pileups. 3D-resolved X-ray micro-diffraction uniquely allows examination of the complex lattice distortions beneath specific indents. In the ion-implanted material we find reduced lattice rotations and residual strains due to indentation, indicating a more confined plastic zone. Together, our observations suggest that helium-induced defects initially act as efficient obstacles to dislocation motion, but are weakened by the subsequent passage of dislocations, causing a reduction in work hardening capacity.

The calculated depth of penetration of the indenter indicates, that for a sample implanted with manganese ions with dose $D=1\cdot10^{17}$ Mn^{+}/cm^{2} this value is more than twice higher than a range of ion implantation from the numerical simulation, and for the remaining samples the depth is three times higher than range resulting from the simulation. This indicates a visible effect of the implanted ions at depths greater than those resulting from the implantation process. In the literature, this phenomenon has been described as a long-range effect of ion implantation [36, 37, 38, 39].

The increase in the load to 5 gf resulted in an increase in the depth of microhardness tester penetration. The mean indexation depth for all the samples exceeded 0.71 um. The results of microhardness measurements are no longer so differentiated between individual samples and the mean value does not differ from the microhardness of the unimplanted sample by more than 5%. The Kruskal-Wallis test didn't show statistically significant differences between the microhardness of individual samples. This indicates a decrease in the significance of ion implantation for changes in the microhardness of the cobalt alloy. The results of the microhardness of individual samples measured at 5 gf load are shown in Figure 5.

CONCLUSIONS

Cobalt alloys defined as Stellites due to their strength properties can be used in the construction of critical machine elements, such as components of combustion engines. In this paper, the influence of manganese and nitrogen ion implantation on the microhardness of cobalt alloy Stellite 6 was investigated. The following conclusions can be drawn:

- both manganese ion implantation with energy E=175 keV and nitrogen ion implantation with energy E=120 keV seems increasing the microhardness of cobalt alloy Stellite 6,
- the highest increase in microhardness was observed for the sample implanted with manganese ions with a dose $D=1\cdot10^{17}$ Mn^{+}/cm^{2},
- the effect of ion implantation on microhardness is noticeable at depths greater than the original range of the implanted ions, which confirms the long-range effect of ion implantation,
- measuring within comparison to the Vickers HV0.001, measuring with HV0.005 scale effects on a greater depth of the indentation, which results in a reduced difference between the microhardness of the implanted and unimplanted samples,
- increased energy of nitrogen ion implantation showed no increase in $HV_{0.005}$ microhardness compared to the results presented in the paper [24],
- the use of ion implantation to improve mechanical properties may be justified in the case of precision machinery and pairs where the importance of tenths of a micrometer is important for the efficient operation of the machine.

Acknowledgments

This research was supported by the National Science Centre (Poland) grant number DEC-2018/02/X/ST8/02653.

REFERENCES

1. Adamiec, P. and Dziubiński, J. Wytwarzanie i właściwości warstw wierzchnich elementów maszyn tranposrtowych. WPŚ: Gliwice 2005.
2. Adamiec, P. and Dziubiński, J. Wybrane zagadnienia materiałów konstrukcyjnych i technologii wytwarzania pojazdów. WPŚ: Gliwice 1998.
3. Moćko, W. Analiza wytężenia zaworu silnikowego wykonanego ze stopu tytanu Ti6Al4V obciążonego mechanicznie i cieplnie. Transport samochodowy 2014, 4, 55–71.
4. Yao, J., Zhang, Q., Kong, F., and Ding, Q. Laser hardening techniques on steam turbine blade and application. Physics Procedia 2010, 5, 399–406.
5. Li, B., Jin, Y., Yao, J., Li, Z., Zhang, Q., and Zhang, X. Influence of laser irradiation on deposition characteristics of cold sprayed Stellite-6 coatings. Optics & Laser Technology 2018, 100, 27–39.
6. Janicki, D. Microstructure and sliding wear behaviour of in-situ TiC-reinforced composite surface layers fabricated on ductile cast iron by laser alloying. Materials 2018, 11.
7. Wang, Z. and Suzuki, T. Friction law in dry metal forming of materials with work hardening. Procedia Manufacturing 2018, 15, 475–480.
8. Hughes, D.A. and Hansen, N. The microstructural origin of work hardening stages. Acta Materialia 2018, 148, 374–383.
9. Żebrowski, R., Walczak, M., Klepka, T., and Pasierbiewicz, K. Effect of the shot peening on surface properties of Ti-6Al-4V alloy produced by means of DMLS technology. Eksploatacja i Niezawodnosc 2019, 21, 46–53.
10. Maruszczyk, A., Dudek, A., and Szala, M. Research into Morphology and Properties of TiO_2 – NiAl Atmospheric Plasma Sprayed Coating. Advances in Science and Technology Research Journal 2017, 11, 204–210.
11. Szala, M. and Hejwowski, T. Cavitation Erosion Resistance and Wear Mechanism Model of Flame-Sprayed Al_2O_3-40%TiO_2/NiMoAl Cermet Coatings. Coatings 2018, 8, 254.
12. Szala, M., Walczak, M., Pasierbiewicz, K., and Kamiński, M. Cavitation erosion and slidingwear mechanisms of AlTiN and TiAlN films deposited on stainless steel substrate. Coatings 2019, 9.
13. Budzyński, P., Kamiński, M., Surowiec, Z., and Skuratov, V.A. Mechanical and electrical properties of the titanium surface layer irradiated with 168

MeV^{136}Xe ions. Przeglad Elektrotechniczny 2018, 94.

14. Budzynski, P., Kara, L., Küçükömeroǂlu, T., and Kaminski, M. The influence of nitrogen implantation on tribological properties of AISI H11 steel. Vacuum 2015, 122, 230–235.
15. Foerster, C. E., Silva, S.L.R. da, Fitz, T., Dekorsy, T., Prokert, F., Kreiβig, U., Richter, E., Möller, W., Lepienski, C.M., and M. Siqueira, C.J. de Carbon ion implantation into aluminium: Mechanical and tribological properties. Surface and Coatings Technology 2006, 200, 5210–5219.
16. Budzyński, P. Problematyka tarcia i zużycia tworzym metalowych implantowanych jonowo w technologii maszyn. Wydawnictwo Politechniki Lubelskiej: Lublin 2010.
17. Zhu, Y.-C., Fujita, K., Iwamoto, N., Nagasaka, H., and Kataoka, T. Influence of boron ion implantation on the wear resistance of TiAlN coatings. Surface and Coatings Technology 2002, 158–159, 664–668.
18. Yan, S., Zhao, W., Rück, D., Xue, J., and Wang, Y.. Study of tribological properties of high-speed steel implanted by high-dose carbon ions. Surface and Coatings Technology 1998, 103–104, 348–352.
19. Burakowski, T. and Wierzchoń, T. Inżynieria powierzchni metali. WNT: Warszawa 1995.
20. Das, S., Armstrong, D.E.J. , Zayachuk, Y., Liu, W., Xu, R., and Hofmann, F. The effect of helium implantation on the deformation behaviour of tungsten: X-ray micro-diffraction and nanoindentation. Scripta Materialia 2018, 146, 335–339.
21. Derry, T. E., Lisema, L.I., Magabe, A.T. , Aradi, E., Machaka, R., and Madhuku, M. Allotrope conversion and surface hardness increase in ion implanted boron nitride. Surface and Coatings Technology 2018, 355, 61–64.
22. Vlcak, P., Cerny, F., Drahokoupil, J., Sepitka, J., and Tolde, Z. The microstructure and surface hardness of Ti6Al4V alloy implanted with nitrogen ions at an elevated temperature. Journal of Alloys and Compounds 2015, 620, 48–54.
23. Picard, S., Memet, J., Sabot, R., Grosseau-Poussard, J., Rivière, J., and Meilland, R. Corrosion behaviour, microhardness and surface characterisation of low energy, high current ion implanted austenitic stainless steel. Materials Science and Engineering: A 2001, 303, 163–172.
24. Budzyński, P., Kamiński, M., Pałka, K., Droździel, A., and Wiertel, M. The influence of nitrogen ion implantation on microhardness of the Stellite 6 alloy. IOP Conference Series: Materials Science and Engineering 2016, 148
25. Ziegler, J.F., Ziegler, M.D., and Biersack, J.P. SRIM – The stopping and range of ions in matter 2010. Nuclear Instruments and Methods in Physics Research Section B: Beam Interactions with Materials and Atoms 2010, 268, 1818–1823.
26. Mohammadi, A., Hamidi, S. and Asadabad, M.A. The use of the SRIM code for calculation of radiation damage induced by neutrons. Nuclear Instruments and Methods in Physics Research Section B: Beam Interactions with Materials and Atoms 2017, 412, 19–27.
27. Saha, U., Devan, K., and Ganesan, S. A study to compute integrated dpa for neutron and ion irradiation environments using SRIM-2013. Journal of Nuclear Materials 2018, 503, 30–41.
28. Hofsäss, H., Zhang, K. and Mutzke, A. Simulation of ion beam sputtering with SDTrimSP, TRIDYN and SRIM. Applied Surface Science 2014, 310, 134–141.
29. Privezentsev, D., Zhiznyakov, A. and Kulkov, Y. Analysis of the Microhardness of Metals Using Digital Metallographic Images. Materials Today: Proceedings 2019, 11, 325–329.
30. Kamiński, M., Budzyński, P., Szala, M. and Turek, M. In Tribological properties of the Stellite 6 cobalt alloy implanted with manganese ions, W., M. Eds.; Institute of Physics Publishing: 2018.
31. Hou, Q.Y. , Gao, J.S. and Zhou, F. Microstructure and wear characteristics of cobalt-based alloy deposited by plasma transferred arc weld surfacing. Surface and Coatings Technology 2005, 194, 238–243.
32. Lin, W.C. and Chen, C. Characteristics of thin surface layers of cobalt-based alloys deposited by laser cladding. Surface and Coatings Technology 2006, 200, 4557–4563.
33. Klonecki, W. Elementy statystyki dla inżynierów. O. Wyd. Politechniki Wrocławskiej: Wrocław 1996.
34. Budzynski, P., Kaminski, M., Wiertel, M., Pyszniak, K. and Droździel, A. Mechanical properties of the stellite 6 cobalt alloy implanted with nitrogen ions. Acta Physica Polonica A 2017, 132, 203–205.
35. Nath, V.C., Sood, D.K. and Manory, R.R. Ultramicrohardness and microstructure of Ti-6 wt.%Al-4 wt.%V alloy nitrided by ion implantation. Surface and Coatings Technology 1991, 49, 510–513.
36. Didenko, A.N., Kozlov, E.V. , Sharkeev, Y.P., Tailashev, A.S., Rjabchikov, A.I., Pranjavichus, L., and Augulis, L. Observation of deep dislocation structures and "long-range effect" in ion-implanted α-Fe. Surface and Coatings Technology 1993, 56, 97–104.
37. Sharkeev, Y. and Kozlov, E. The long-range effect in ion implanted metallic materials: dislocation structures, properties, stresses, mechanisms. Surface and Coatings Technology 2002, 158–159, 219–224.
38. Sharkeev, Y.P., Kozlov, E.V., Didenko, A.N., Kolupaeva, S.N. and Vihor, N.A. The mechanisms of the long-range effect in metals and alloys by ion implantation. Surface and Coatings Technology 1996, 83, 15–21.
39. Budzyński, P., Kamiński, M., Droździel, A. and Wiertel, M. Long-range effect of ion implantation of Raex and Hardox steels. IOP Conference Series: Materials Science and Engineering 2016, 148.